Fermi surface of an important nano-sized metastable phase: Al_3Li

J. Laverock,[1] S.B. Dugdale,[1] M.A. Alam,[1] M.V. Roussenova,[1] J. Wensley,[1] J. Kwiatkowska,[2] and N. Shiotani[3]

[1]*H. H. Wills Physics Laboratory, University of Bristol, Tyndall Avenue, Bristol BS8 1TL, United Kingdom*

[2]*H. Niewodniczański Institute of Nuclear Physics, Polish Academy of Sciences, Radzikowskiego 152, 31-342 Kraków, Poland*

[3]*KEK-PF, Tsukuba, Ibaraki 305-0801, Japan*

Nanoscale particles embedded in a metallic matrix are of considerable interest as a route towards identifying and tailoring material properties. We present a detailed investigation of the electronic structure, and in particular the Fermi surface, of a nanoscale phase ($L1_2$ Al_3Li) that has so far been inaccessible with conventional techniques, despite playing a key role in determining the favorable material properties of the alloy (Al-9 at. %-Li). The ordered precipitates only form within the stabilizing Al matrix and do not exist in the bulk; here, we take advantage of the strong positron affinity of Li to directly probe the Fermi surface of Al_3Li. Through comparison with band structure calculations, we demonstrate that the positron uniquely probes these precipitates, and present a 'tuned' Fermi surface for this elusive phase.

arXiv:1009.2265v1 [cond-mat.mtrl-sci] 12 Sep 2010

In recent years, many of the properties of the Al-Li alloy system have come under careful scrutiny, not least because of the widespread interest in these materials by the aerospace industry. In the Al-rich region of the phase diagram (Li concentrations between 5% and 25%), these alloys offer high stiffness and superior strength-to-weight ratios, principally due to the hardening which occurs through the precipitation of nanoscale particles. The Li-rich strengthening precipitates, known as the δ' phase, are Al_3Li and are highly ordered with an $L1_2$ structure, and remain crystallographically coherent with the parent (face-centered cubic, fcc) solid-solution matrix with small lattice mismatch [1, 2]. The size of the precipitates, and the volume they occupy, depend not only on the Li concentration, but also the particular conditions experienced (such as heat treatment and ageing) [3]; for the Al-9at.%Li samples considered here, that volume is approximately 20%, comprising roughly spherical precipitates with an average diameter of about 20nm.

However, the δ' phase is metastable [2], and only exists within the parent Al fcc matrix. For this reason, knowledge of the electronic structure of the Al_3Li precipitates has so far only come from band-theoretical calculations (see, for example, [4]). Although some of the strengthening qualities orginate from the fact that the precipitates act as pinning centres for defects, it is believed that Al_3Li has a particularly high Young's modulus, which, of course, stems from its electronic structure [5, 6].

Advantage is taken in this study of the strong positron affinity of Li-rich regions [7] to directly probe the electronic structure (in the form of its Fermi surface) of the δ'-phase Al_3Li precipitates. Here, the strong positron affinity leads to the trapping of most of the positrons in the precipitates facilitating an unambiguous probing of the properties of the precipitates alone since the experimental signatures are sufficiently different from the host matrix. Previous pioneering positron studies of nanoscale precipitates [8, 9] (and even quantum dots [10]) have, for a variety of reasons, restricted their analyses to p-space rather than k-space. Here, the Fermi surface (FS) of the precipitate itself is the objective.

Positron annihilation is a well-established technique for investigating the occupution densities in k-space, and hence the FS, which is accessed via the momentum distribution measured by the 2-Dimensional Angular Correlation of electron–positron Annihilation Radiation (2D-ACAR) technique [11]. A 2D-ACAR measurement yields a 2D projection (integration over one dimension) of the underlying electron-positron momentum density, $\rho^{2\gamma}(\mathbf{p})$, in which the FS is expressed through discontinuities in the distribution at the Fermi momenta $\mathbf{p}_F = \mathbf{k}_F + \mathbf{G}$, where $\mathbf{k}_F$ represent the loci of the FS in k-space and $\mathbf{G}$ is a vector of the reciprocal lattice. When the FS is of paramount interest, the application of the Lock-Crisp-West (LCW) procedure [12] is used to superimpose the contribution from successive Brillouin zones (BZ) into the first BZ, thereby directly providing a map of the projection of the occupied states in the BZ (i.e. a projection of the FS).

In order to assess the topology of the measured FS, positron annihilation (2D-ACAR) measurements have been combined with *ab initio* electronic structure calculations. The aim of this combined approach is to: (a) establish that the measured Fermi surface indeed arise from the precipitates alone and (b) obtain as accurate a picture as possible of the first experimental FS of the Al_3Li phase. To achieve these goals, first of all, we consider the annihilation of the positron, and in particular its sensitivity to the ordered precipitates, by considering all possible scenarios: i) the positron annihilates *only* with delocalized electrons in the δ' precipitates, and our measured FS is that of $L1_2$ Al_3Li, ii) the positron annihilates with the Al matrix, and our measured FS resembles pure Al, iii) the positron annihilates from both the Al_3Li precipitates *and* the Al matrix, and our FS measurement is a weighted average of both, iv) our measurements reflect the stoichiometry of the sample, and the FS resembles that of the disordered alloy $Al_{0.91}Li_{0.09}$. Electronic structure calculations of pure Al and Al_3Li have been performed using the linear muffin-tin orbital (LMTO) method [17],

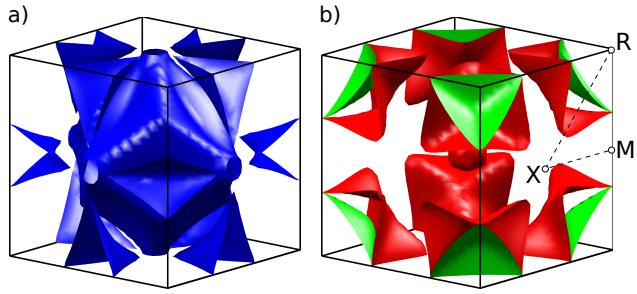

FIG. 1: The hole (a) and two electron (b) FS sheets of Al_3Li predicted by the LMTO calculation. The symmetry points of the BZ are labelled in (b); the Γ-point is at the centre.

whereas for the disordered $Al_{0.91}Li_{0.09}$ and $Al_{0.75}Li_{0.25}$ alloys, the Korringa-Kohn-Rostoker (KKR) within the coherent potential approximation (CPA) framework [18] was employed. Full-potential calculations (using the Elk code [23]) have also been performed to investigate any inaccuracies associated with the potential shape approximations employed by the LMTO and KKR implementations. The LMTO calculations predict three FS sheets for $L1_2$ Al_3Li, shown in Fig. 1, the first of which is a hole sheet (enclosing unfilled states) and the second and third are both electron sheets (enclosing filled electron states). Note that all FS sheets enclose filled states (and are therefore occupied) at the R-point (corner) of the BZ. These calculations agree well with previous calculations [4], as well as with our additional KKR and Elk calculations (not presented here). Moreover, the Elk calculations yield a large (zero-temperature) Young's modulus of 137 GPa, in excellent agreement with the findings of Ref. [5].

A single crystal of the Al-Li alloy was grown by the Bridgman method from high purity Al (99.999%) and Li (99.95%) by adding Li into molten Al, followed by stirring and casting, sealed within a stainless steel capsule under an Ar pressure of 3 atm. to prevent excessive loss of Li during the crystallisation process. The final Li content in the single crystal was determined by Atomic Absorption Spectrometry and independently in each sample by Proton Induced Gamma Emission and was found to be 9 at.%. The crystal was oriented using Laue back-reflection and specimens of 1.5 mm thickness were cut along planes normal to the main crystallographic directions. The usual procedure of alternate mechanical polishing and chemical polishing was applied to remove damaged surface layers. Separate measurements on the same samples of the positron lifetime [13] indicate that the positron is fully trapped in (and therefore annihilates from) the Al_3Li δ' precipitates [14], already hinting at scenario (i) outlined above.

A series of 2D-ACAR measurements along four different crystallographic directions ([100], [110], [111] and [210]) were made on the Bristol spectrometer (with a resolution function of 0.16×0.19 $(2\pi/a)$ in the x and y data axes respectively) and analysed in order to obtain the projected electron-positron momentum density in the first BZ, shown in Fig. 2 (in the absence of positron effects, this would simply correspond to the occupation density in the first BZ). The sensitivity of our data to the FS is immediately obvious: Strong regions of high momentum (occupation) density are observed near the projected R-points of the BZ, at which each sheet of FS is fully occupied. To accompany these measurements, the 3D electron-positron momentum density was computed from our electronic structure calculations and the projected (2D) density in the first BZ was obtained for each corresponding projection.

We begin with a visual comparison of the measured quantities and their corresponding theoretical distributions. Good agreement is already observed between the data and the IPM LMTO calculations of Al_3Li shown in Fig. 2. However, in order to eliminate the possibility that the positron is sampling the Al matrix rather than the δ' precipitates (scenario ii), both experimental and theoretical distributions were also obtained of pure Al along two crystallographic projections ([110] and [111]), shown in Fig. 3 in the same $L1_2$ BZ of Al_3Li. Unsurprisingly, good agreement is observed between experiment and theory for Al, but there are stark differences between the Al distributions and our experimental data for Al-9 at. %-Li. In the [110] projection (comparing Figs. 2b and 3a), the most obvious differences are in the shape of the projected FS near RX, as well as the distribution near ΓM and X. For the [111] projection (comparing Figs. 2c and 3b), the shape of the distribution, particularly near MX, is markedly different. These results strongly suggest that the positron is, indeed, sensitive to the Li-rich regions of the crystal, rather than the Al matrix. In fact, linear combinations of the distributions of the pure Al and $L1_2$ Al_3Li calculations were not found to improve the agreement between experiment and theory over the Al_3Li calculations alone, eliminating scenario iii) and further suggesting that *all* of the positrons annihilated from the Li-rich precipitates, in agreement with independent positron lifetime measurements on the same samples [13].

In order to address the final alternative possibility (scenario iv), i.e. that the positron is sampling a *disordered* alloy of the sample stoichiometry, KKR-CPA calculations (also employing the IPM) have been performed for disordered $Al_{0.91}Li_{0.09}$, and are shown in Fig. 4 for two different projections (namely [110] and [111]) in the right panels. For the [110] direction of our data shown in Fig. 2b, the lowest density is observed at X, and there is a weak peak at ΓM, a feature that is well-reproduced by our LMTO calculations. In contrast, for the $Al_{0.91}Li_{0.09}$ calculation (Fig. 4a), the minimum density is located at ΓM, and the shape of the feature at RX is substantially different. Further inspection of the [111] projection (comparing Figs. 2c and 4b) yields similar conclusions, leading us to eliminate this scenario. Finally, we can consider the possibility that, although the measurements are sensitive to the precipitate phase, the precipitates themselves may not be ordered. However, comparisons

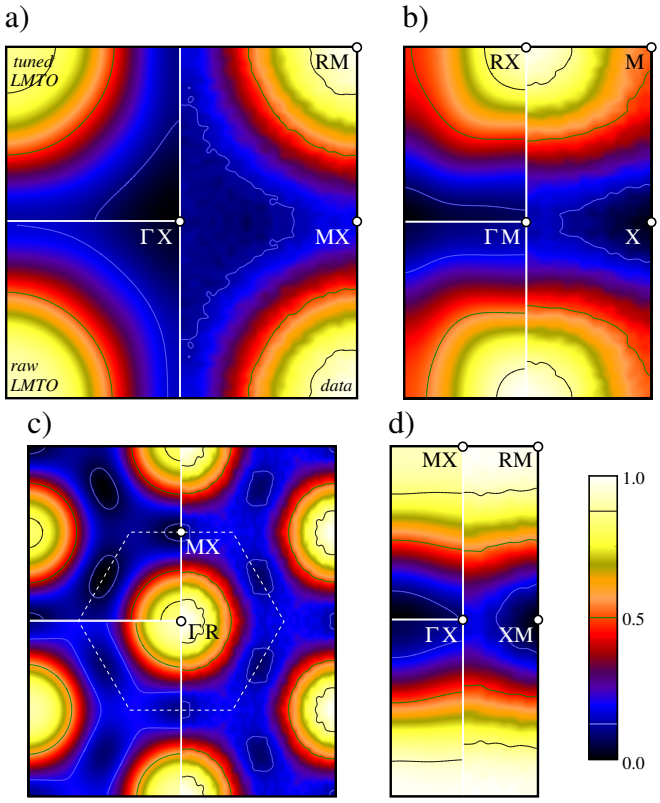

FIG. 2: Positron annihilation data in the first BZ for Al-9 at. %-Li, shown in the right panel, projected along the (a) [100], (b) [110], (c) [111] and (d) [210] crystallographic directions. The high-symmetry points in projection have been labelled, and the projected BZ is marked by the dotted line in (c). In the bottom left panel, the raw LMTO momentum density is shown, and the tuned calculation is presented in the top left panel.

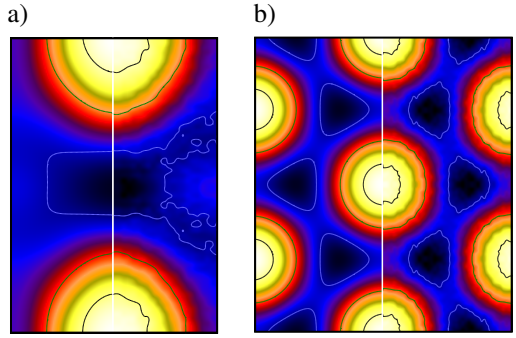

FIG. 3: LMTO (left panels) and 2D-ACAR data (right panels) for pure Al, shown in the $L1_2$ BZ projected along the (a) [110] and (b) [111] crystallographic directions.

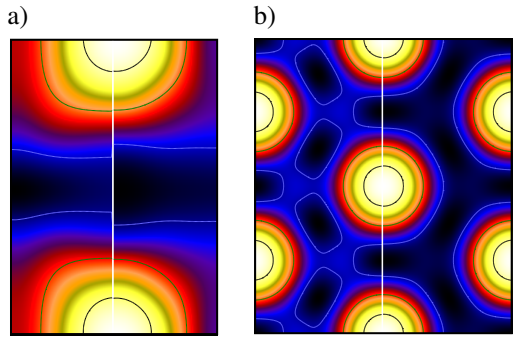

FIG. 4: KKR-CPA calculations of the momentum distribution of disordered $Al_{0.75}Li_{0.25}$ (left panels) and $Al_{0.91}Li_{0.09}$ (right panels) projected along the (a) [110] and (b) [111] directions.

with a KKR-CPA calculation of disordered $Al_{0.75}Li_{0.25}$, shown in the left panels of Fig. 4, although superficially similar, are quantitatively in poorer agreement with the data than the ordered Al_3Li calculations. This is most obvious in the strength of the peaks near ΓM for the [110], and near the corner of the projected BZ boundary for the [111] projection. Together with the comparisons with the LMTO calculations of Al_3Li and the pure Al measurements, this leads us to our first conclusion: that the positron is sampling the Li-rich δ' precipitate phase of ordered $L1_2$ Al_3Li.

In terms of the FS topology, the agreement between the data and LMTO Al_3Li calculations, although already very good, can be 'tuned' by rigidly shifting the theoretical bands, culminating in a fitted FS whose overall shape more resembles the experimental FS. This approach has already been successfully applied in p-space to both positron [15] and Compton scattering [21] data. Here, we operate in k-space, and employ the state-dependent enhancement scheme outlined in Ref. [22]. This method, including the site- and orbital-specific annihilation rates to the positron enhancement as fitting parameters, has been shown to improve the agreement between theory and high-precision data on the FS of a variety of elemental metals, as well as providing a measurement of the positron enhancement itself [22].

The results of the rigid-band fit, as expected, reflect the higher positron affinity of Li over Al, with the positron preferentially annihilating from within the Li atomic sphere (34.6%) rather than the equally-sized Al atomic sphere (21.8% $\times$ 3). Indeed, this site-dependence is already well-accounted for by the LDA calculation of the positronic state, which predicts 35.2% and 21.6% respectively for the Li and Al sites. The state-dependent enhancement factors (see Ref. [22]) demonstrate the de-enhancement of p states (by a factor 0.59) and d states (by a factor 0.43) relative to the s states that has previously been observed for transition metals and semiconductors [16, 19].

Firstly, the rigid-band fit is found to be sensitive to all of the FS sheets, unambiguously confirming their presence. The bands are found to shift upwards in energy (becoming less occupied) by $\sim$ 50 mRy, and lead to a 'tuned' FS, shown in Fig. 5. It is emphasized that there are no constraints to these parameters, meaning that each sheet of FS is individually free to be completely empty or fully occupied, or indeed any shape in between

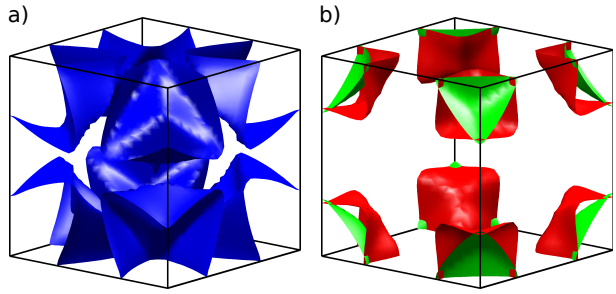

FIG. 5: The FS obtained by tuning our LMTO calculation (by rigidly shifting each band) of Al_3Li to the experimental data (compare with Fig. 1).

allowed by its band structure. Although the shifts are quite large, the bands are of predominantly p character and have large Fermi velocities (energy gradients), and so the modification (in k-space) to the Fermi breaks themselves is weaker. Indeed, we find that this shift in the Fermi wave vector is $\Delta k_{\rm F} \sim 0.05 - 0.08$ $(2\pi/a)$, which is less than half of the experimental resolution function. Nonetheless, these shifts still correspond to a total reduction in the number of occupied states of ~ 0.84 electrons. The most plausible interpretation of these results is that the topology of the experimental FS more closely resembles that shown in Fig. 5 than the raw LMTO calculation of Fig. 1. In previous studies, the present fitting method has been found to improve the description of the FS (in comparison with high-precision quantum oscillation measurements) in all the systems investigated (including Al) [22]. Moreover, the LDA is well-known to place the d bands (unoccupied in Al_3Li) too low with respect to sp bands in transition metals [20]. Our raw LMTO calculations of Al_3Li predict an appreciable hybridization with these unoccupied d states, having 26 % total d character at $E_{\rm F}$. In the rigid-band fit, however, this quantity is somewhat reduced, as the sp bands below $E_{\rm F}$ and d bands above $E_{\rm F}$ are pushed apart. The results of the fit can be interpreted as a reaction to the over-estimation by the LDA of the hybridization between the sp and d states, where the flatter d bands, over-estimated at $E_{\rm F}$, impact on the topology of the FS. Since the computation of the elastic constants can only be performed at the minimum of the LDA, the impact these results might have on the predicted material properties of Al_3Li (such as its Young's modulus) remains open to investigation.

In summary, we have successfully measured the FS of a nano-sized metastable phase of matter, previously inaccessible using conventional techniques. By taking advantage of the positron affinity of Li, our 2D-ACAR measurements of Al-9 at. %-Li yield a momentum density in close agreement with electronic structure calculations of ordered $L1_2$ Al_3Li, corresponding to the δ' precipitates. Moreover, comparisons with theoretical distributions of pure Al as well as of the disordered alloys $Al_{0.91}Li_{0.09}$ and $Al_{0.75}Li_{0.25}$ eliminate other plausible fates of the positron, firmly establishing the positron as a unique probe of the δ' precipitates. Detailed subsequent analysis of the momentum density, including the application of a novel rigid-band fitting method that additionally accounts for the state-dependent positron enhancement, has yielded a 'tuned' FS for this elusive phase.

[1] B. Noble and G.E. Thompson, Metal Sci. **5**, 114 (1971); S.F. Baumann and D.B. Williams, Scrita Metall. **18**, 616 (1984); K. Mahalingham *et al.*, Acta Metall. **35**, 483 (1987).
[2] M. Sluiter *et al.*, Phys. Rev. B **42**, 10460 (1990).
[3] M.E. Krug, D.C. Dunand and D.N. Seidman, Appl. Phys. Lett. **92**, 124107 (2008); V. Radmilovic *et al.*, Scr. Mater. **58**, 529 (2008).
[4] X.-Q. Guo *et al.*, Phys. Rev. B **41**, 12432 (1990).
[5] X.-Q. Guo, R. Podloucky and A.J. Freeman, J. Mater. Res. **6**, 324 (1991).
[6] A. Mikkelsen *et al.*, Phys. Rev. Lett. **87**, 096102 (2001).
[7] M.J. Puska, P. Lanki and R.M. Niemenen, J. Phys. Condens. Matter **1**, 6081 (1989).
[8] Y. Nagai *et al.*, Phys. Rev. Lett. **87**, 176402 (2001); Y. Nagai *et al.*, Phys. Rev. B **79**, 201405(R) (2009).
[9] P. Asoka-Kumar *et al.*, Phil. Mag. Lett. **82**, 609 (2002).
[10] S.W.H. Eijt *et al.*, Nature Mater. **5**, 23 (2006).
[11] R.N. West, in *Proceedings of the International School of Physics <<Enrico Fermi>> — Positron Spectroscopy of Solids*, edited by A. Dupasquier and A.P. Mills, jr. (IOS Press, Amsterdam, 1995).
[12] D.G. Lock, V.H.C. Crisp and R.N. West, J. Phys. F **3**, 561 (1973).
[13] The lifetime measurements were performed by J. Dryzek.
[14] J. Del Rio, F. Plazaola and N. De Diego, Philos. Mag. A **69**, 591 (1994)
[15] Zs. Major *et al.*, Phys. Rev. Lett. **92**, 107003 (2004); Zs. Major *et al.*, J. Phys. Chem. Solids **65**, 2011 (2004).
[16] T. Jarlborg and A.K. Singh, Phys. Rev. B **36**, 4660 (1987).
[17] B. Barbiellini, S.B. Dugdale and T. Jarlborg, Comp. Mater. Sci. **28**, 287 (2003).
[18] H. Ebert, *Electronic Structure and Physical Properties of Solids*, ed. H. Dreyssé, Lecture Notes in Physics **535**, Springer, Berlin (1998), 191; `http://olymp.cup.uni-muenchen.de/ak/ebert/SPRKKR/`
[19] B. Barbiellini *et al.*, Phys. Rev. B **56**, 7136 (1997).
[20] S. Wakoh and J. Yamashita, J. Phys. Soc. Jpn. **35**, 1394 (1973); H. Eckardt, L. Fritsche, and J. Noffke, J. Phys. F **14**, 97 (1984).
[21] C. Utfeld *et al.*, Phys. Rev. Lett. **103** 226403 (2009); C. Utfeld *et al.*, Phys. Rev. B **81** 064509 (2010).
[22] J. Laverock *et al.*, arXiv: 1005.4909v1 (2010).
[23] J.K. Dewhurst *et al.*, `http://elk.sourceforge.net` (2009).